Collinear quasiclassical trajectory study of collision-induced dissociation on a model potential energy surface[a)]

Jack A. Kaye[b)] and Aron Kuppermann
Arthur Amos Noyes Laboratory of Chemical Physics,[c)] California Institute of Technology, Pasadena, California 91125

(Received 29 March 1985; accepted 10 October 1985)

Quasiclassical trajectory calculations have been carried out at energies above the threshold for collision-induced dissociation for a model symmetric collinear atom–diatomic molecule system. Exact quantum mechanical calculations have shown that quasiclassical trajectories give a qualitatively correct picture of the dynamics in this system, in so far as reaction and total dissociation probabilities are concerned. Trajectories leading to dissociation are found to lie almost entirely in well-defined reactivity bands, with the exception of a few occurring in a small chattering region in which the outcome of the trajectory is extremely sensitive to its initial conditions. The energy distribution functions of the dissociated atoms are obtained and shown to vary substantially with initial conditions (reagent vibrational and translation energy). The form of these distributions is, to a major extent, determined by the position and width of the reactivity bands. The different dissociation reactivity bands are shown to be associated with different types of trajectories. Part of the vibrational enhancement of dissociation arises from the fact that the simplest possible trajectory leading to dissociation (one which crosses the symmetric stretch line only once prior to the onset of dissociation) is not obtained with ground state reagents.

I. INTRODUCTION

The collision-induced dissociation (CID) of diatomic molecules

$$A + BC \rightarrow A + B + C \tag{1}$$

is a process of great fundamental interest in chemistry, particularly at the high temperatures associated with shock waves, both in the laboratory[1] and in interstellar space.[2] The *ab initio* calculation of CID rates has proven to be extremely difficult, as one must have accurate methods for calculating the potential energy surface for the collision, solving for the dynamics, and then integrating the coupled rate equations to obtain expressions for the rate of disappearance of the diatomic molecule.

The development of accurate methods for solving for the dynamics has been especially difficult. Kinematic and quasiclassical trajectory (QCT) calculations have been extensively used to study CID.[3] The number of studies incorporating quantum mechanical effects, either by a semiclassical or a purely quantum mechanical approach, is much smaller.[4–11] Most of these studies have been restricted to collinear collisions in which reactive processes of the type

$$A + BC \rightarrow AB + C \tag{2}$$

are not permitted. Noncollinear collisions in nonreactive systems have been studied by a semiclassical method by Rusinek.[5(a)] There have been published, however, three purely quantum calculations in which reaction and dissociation were allowed to compete, all of them for collinear collisions: the wave packet approach pioneered by Kulander,[6,10(b)] the hyperspherical coordinate coupled-channel method developed independently in our laboratories,[7] and by Hauke, Manz, and Römelt,[8] and the multiple collision approach of Beard and Micha[9] (which has been applied to a nonreactive system).

The availability of accurate quantum mechanical (QM) results for CID has increased interest in QCT studies. In particular, Kaye and Kuppermann[7(b)] have shown that for the collinear model system they studied, the QCT results for the reaction probabilities and the total CID probabilities were qualitatively similar to the QM ones. Since the model system involves light masses (each of the atoms A, B, C have a mass equal to that of a hydrogen atom) and weakly bound (by 0.22 eV) molecules, quantum effects might be expected to be important. This suggests that QCT calculations might be useful predictors of the gross features of CID in reactive systems. Good agreement between CID probabilities from semiclassical[5(b)] and quantum mechanical[4(c)] calculations for a model collinear nonreactive system has also been reported. One must approach this with some caution, however, as in a different nonreactive system, Gray *et al.*[10(a)] have obtained major differences in the dissociation probability between their QCT results and the QM results of Knapp and Diestler[11] for the same system.

In order to help gain a better understanding of the dynamics of this model system, we describe in this paper a reactivity band analysis of the QCT results. Reactivity bands are those regions of the two-dimensional space spanned by the system's energy and the initial diatomic reagent vibrational phase in which the outcome of the collision (chemical reaction, dissociation, or nonreaction) is the same.

Such analyses have been extensively applied to collinear reactive systems below dissociation[12,13] and have also been applied to a collinear nonreactive system above dissociation.[10(a)] A classical phase space analysis of CID in such a

[a)] This work was supported in part by a contract (No. F49620-79-C-0187) from Air Force Office of Scientific Research.

[b)] Work performed in partial fulfillment of the requirements for the Ph. D. degree in Chemistry at the California Institute of Technology. Present Address: NASA Goddard Space Flight Center, Code 616, Greenbelt, MD 20771.

[c)] Contribution No. 7011.

 0021-9606/86/031463-14$02.10

system has recently been performed.[14(a)] We examine bandedness in the plots of trajectory outcome (reaction, nonreaction, dissociation) as a function of initial vibrational phase of the diatomic molecule and the relative kinetic energy. A discussion of the regions separating nonreactive, dissociative, and reactive bands for the collinear $H + H_2$ system has also been published recently.[14(b)]

We also consider the variation of the vibrational action of the diatomic product of nonreactive and reactive collisions with initial vibrational phase. In dissociative collisions we examine how the partitioning of the energy among the three product atoms varies with initial vibrational phase and reagent translational energy. We also examine individual trajectories in order to understand the origin of the reactivity bands.

II. CALCULATION PROCEDURE

The QCT calculations have been performed using standard methods.[15] The model potential energy surface used has been described previously[7(b)]; we repeat here its basic features. It is of the rotating Morse-cubic spline type[16] and has asymptotic Morse oscillator parameters[17] of $D_e = 0.22$ eV, $R_{eq} = 1.400\,83$ bohr, and $\beta = 1.6$ bohr^{-1}. There is a barrier to exchange of 0.14 eV. Equipotential contours of this surface are plotted, together with selected trajectories, in several of the figures in this paper (see Sec. IV). A schematic diagram showing the features of this potential energy surface along its minimum energy path and the energy levels of the two vibrational states is presented in Fig. 1.

The trajectories were obtained with an integration time step of 5.41×10^{-17} s. Energy was conserved to four digits in these calculations. Integration of trajectories began with the distance from the incident atom to the center of mass of the diatomic molecule at 12 bohr.

To determine dissociation probabilities and rough boundaries for reactivity bands, we initially calculated 100 trajectories per energy at regularly spaced values of the initial vibrational phase Φ. At selected energies, we substantially narrowed the phase grid near the boundaries of the reactivity bands. Below dissociation we calculated 50 trajectories per energy at regularly spaced ($\pi/25$ rad) values of the initial vibrational phase and subsequently narrowed the grid near the band boundaries.

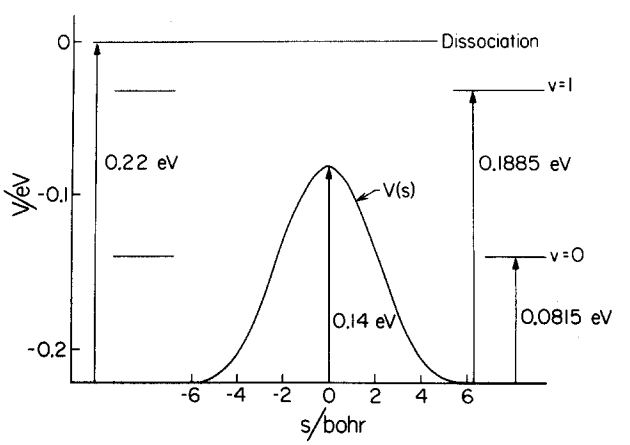

FIG. 1. Schematic diagram of the potential energy function characteristics along the minimum energy path. s is the distance along the path measured from the saddle point configuration, and $V(s)$ is the corresponding potential energy. The horizontal lines indicate the energy levels of the bound states of the isolated diatomic molecules and of the dissociated configuration.

We have also determined the partitioning of kinetic energy among the atoms after the collision. The quantity of greatest interest is the fraction f_X^D (X = A, B, C) of the available kinetic energy E' (the energy of the system with respect to the three infinitely separated atoms at rest) in dissociative collisions in each of the atoms at the end of the collision. [This quantity is labeled E in Refs. 7(b) and 7(d).] In dissociative collisions, the collision was defined to be over when both internuclear distances R_{AB} and R_{BC} were greater than 6.0 bohr and were increasing with time. The sums of the kinetic and potential energies of the AB and BC pairs were each required to be greater than D_e. The corresponding fractions f_A^N for atom A in nonreactive collisions and f_C^R for atom C in reactive collisions are defined similarly. In these cases, the available kinetic energy is defined as the difference between the total energy and the potential energy (measured with respect to the bottom of the isolated diatomic molecule well) when the trajectory was terminated. Plots of these quantities vs initial vibrational phase will connect smoothly to the f_A^D and f_C^D curves across the boundary of the reactivity bands. From the fractional energy vs initial vibrational phase data, one may calculate the probability $(dP_{f_A}^v)_c$ of the fractional kinetic energy f_A of atom A after dissociation being in the range $f_A + df_A$ for a collision in which the diatomic molecule is initially in state v. It is connected to the slope of the curve relating the initial vibrational phase Φ_v (in radians) which gives rise to a dissociative trajectory to the final atom A fractional kinetic energy by

$$(dP_{f_A}^v)_c = df_A \frac{\pi}{2} \sum_i |(d\Phi_v/df_A)_i|. \tag{3}$$

The summation extends over all of the separate regions of initial phase giving rise to dissociation known as dissociative phase segments. The subscript c emphasizes the classical nature of this probability. The $(\frac{1}{2}\pi)$ factor is included so that $(dP_{f_A}^v)_c$ will be appropriately normalized:

$$\int_{f_A^{\min}}^{f_A^{\max}} (dP_{f_A}^v)_c = (P_v^D)_c, \tag{4}$$

where $(P_v^D)_c$ is the total dissociation probability for a molecule initially in state v. The limits of integration in Eq. (4), $f_A^{\min}$ and $f_A^{\max}$, can easily be shown to be given by[18]

$$f_A^{\min} = \frac{m_B + m_C}{m_A + m_B + m_C} \frac{m_A m_C}{m_A m_C + m_B(m_A + m_B + m_C)}, \tag{5a}$$

$$f_A^{\max} = \frac{m_B + m_C}{m_A + m_B + m_C}. \tag{5b}$$

For the system being considered, they lead to $f_A^{\min} = 1/6$ and $f_A^{\max} = 2/3$. As a result of Eqs. (3) and (4) we have

$$(P_v^D)_c = \frac{1}{2\pi} \sum_i (\Delta\Phi_v)_i, \tag{6}$$

where $(\Delta\Phi_v)_i$ is the width of the dissociative phase segment i.

The evaluation of the derivative in Eq. (3) is complicated by the possibility of minima or maxima in the f_A vs Φ curves

which permits $\Phi(f_A)$ to be a multiple valued function of f_A. We separate those regions in which $d\Phi/df_A$ is positive and negative and then separately obtain the derivatives by a three-point finite difference procedure. The resulting derivatives are then used as the input for a cubic spline procedure which permits their calculation as a function of f_A. We next sum the absolute values of the derivatives over all branches of each dissociative reactivity band and over all such dissociative reactivity bands, and divide by 2π for normalization purposes. The resulting curve (called a partitioning probability curve) may contain some numerical noise associated with the numerical differentiation procedures; we have visually smoothed these as well as the spline-induced oscillations.

III. RESULTS

We have studied collisions up to energies beyond twice the dissociation energy. In this energy range both reaction and dissociation occur. Plots of the reaction and dissociation probability vs initial relative translational energy E_v are shown for initial reagent states $v = 0$ and $v = 1$ (the only ones possible) in Figs. 2 and 3, respectively. For both initial reagent states, the reaction probability is zero below a threshold energy, increases rapidly with energy to a large value (0.86 for $v = 0$, 0.96 for $v = 1$), and then decreases to zero (for $v = 0$) or a value just above zero ($v = 1$). It then increases monotonically with energy. The dissociation probabilities for the $v = 0$ and $v = 1$ reagents behave quite differently from each other, however. In the $v = 0$ case, no dissociation is observed until F_0 is substantially (0.08 eV) above its energetic threshold; as the energy increases beyond that, the probability increases slowly, reaching a value of 0.27 at the highest energy studied. For the $v = 1$ case, dissociation sets in at 0.02 eV above its energetic threshold, increases rapidly with energy to a maximum of 0.33 and then decreases rapidly to 0.02 before again increasing with energy up to a value 0.39 at the highest energy studied. It should be emphasized that all of these results are qualitatively similar to the exact quantum mechanical results for this system presented in Ref. 7(b).

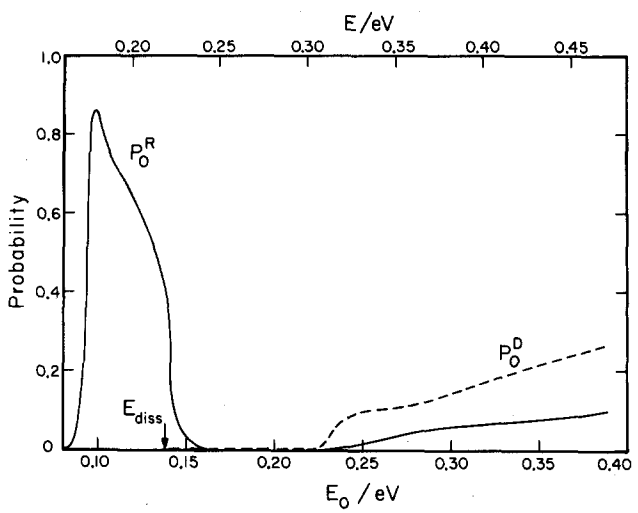

FIG. 2. Probabilities for reaction P_0^R (solid line) and dissociation P_0^D (dashed line) in collisions of ground vibrational state molecules as determined by quasiclassical trajectory calculations as a function of the collision energy. The reagent translational energy E_0 is indicated on the lower abscissa; the total energy E (sum of the vibrational energy—measured with respect to the bottom of the isolated diatom potential energy well—and the translational energy) is indicated on the upper abscissa. The arrow points to the energy at which the dissociation channel becomes energetically accessible. The detailed nature of the reaction probability curve close to threshold is only approximately correct due to the limited number of trajectories computed in that energy region.

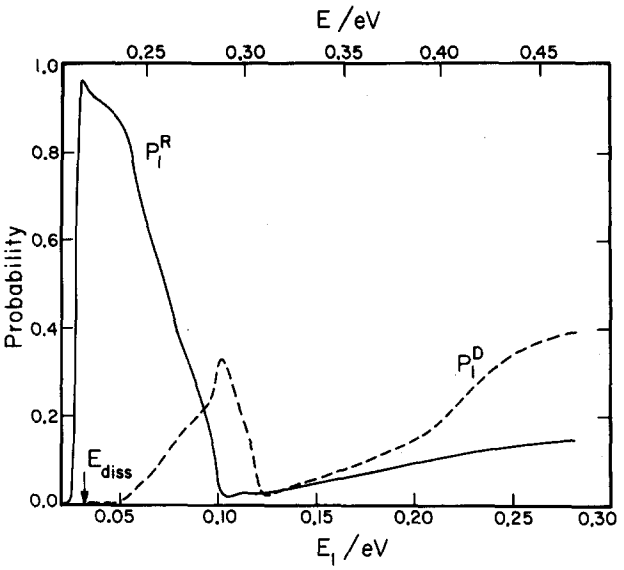

FIG. 3. Probabilities for reaction P_1^R (solid line) and dissociation P_1^D (dashed line) in collisions of vibrationally excited molecules as a function of the reagent translational energy E_1, and total energy collision energy E. (See Fig. 2 caption for details.)

We next examined bandedness in plots of trajectory outcome vs initial vibrational phase and relative translational energy. Plots of the reactivity bands for this system are shown in Figs. 4 and 5 for reagent states $v = 0$ and 1, respectively, for energies above the threshold for CID. Unlike reactivity band plots normally used in studies of reactive atom–diatomic molecule collisions at energies below dissociation,[12,13] in which there are only two possible outcomes of a trajectory (reaction or nonreaction), there are three possible outcomes here: reaction (R), indicated by shaded regions of the figures; dissociation (D), indicated by the speckled regions, and nonreaction (N), indicated by the clear regions. The dissociative band centered near 2.0 rad and 0.17 eV

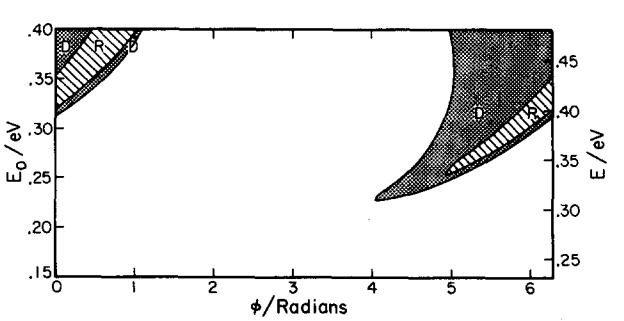

FIG. 4. Reactivity band plot for reaction and dissociation in collisions of ground state molecule. Reactive (R) bands are indicated by shading; dissociative (D) bands are indicated by speckling. The solid white region is nonreactive (N). Both the translational energy E_0 (left ordinate) and the total energy E (right ordinate) are indicated. E is defined in the caption for Fig. 2.

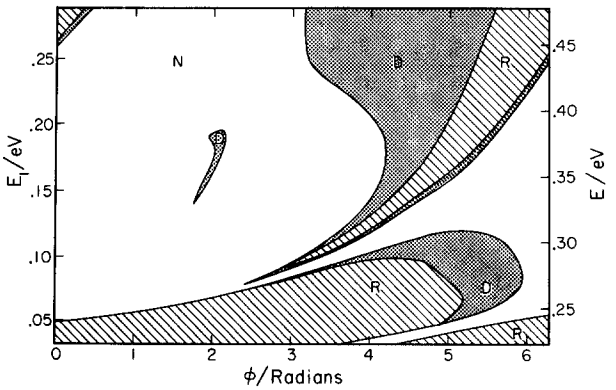

FIG. 5. Reactivity band plot for reaction and dissociation in collisions of vibrationally excited molecules. Band type is indicated as in Fig. 4. Axis labeling is also as in Fig. 4. No effort is made to accurately portray the band structure in the chattering region. (See the text.)

translational energy for $v = 1$ in Fig. 5 is enlarged in Fig. 6.

Fairly well-defined bands are seen to exist above dissociation. When one decreases the difference between neighboring initial phases substantially (to about 0.002 rad), one may find blurring of the boundaries and formation of a "chattering" region[13,19,20(a),21] in which the outcome of the trajectory varies strongly with small changes in the initial phase. This effect is most severe below 0.10 eV translational energy in the $v = 1$ case, where the high energy reaction and dissociation bands come to a cusp (see Fig. 5). For example, at 0.085 eV initial reagent translational energy, between 2.50 and 2.70 rad initial phase, there are four separate dissociative segments, two reactive segments, and one nonreactive segment obtained when the grid spacing of 0.002 rad is used. The total width of all the dissociative segments in this region is 0.052 rad. The dissociation probability produced by this region is only 0.8%, which is far smaller than the contribution at this energy from the large band centered at 5.5 rad. Chattering is also seen near the boundary between reactive and nonreactive bands at energies below dissociation.

We next consider the variation of the vibrational energy of the diatomic molecule resulting from reactive or nonreactive collisions. Normally, to examine this quantity one pre-

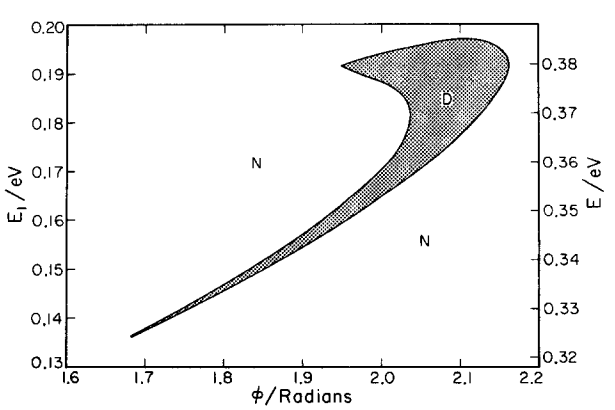

FIG. 6. Enlarged view of the small dissociative band (from Fig. 4) in collisions of vibrationally excited molecules. All markings and axes are as in Fig. 4.

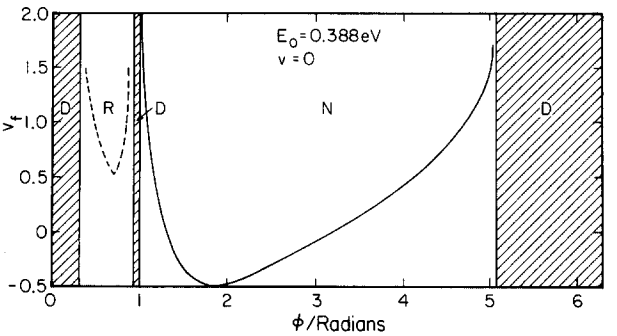

FIG. 7. Final action v_f as a function of the initial phase Φ for a collision involving a ground state diatomic molecule at a reagent translational energy E_0 of 0.388 eV. A solid line is used to connect results of nonreactive trajectories; a dashed line is used to connect results of reactive trajectories. The shaded areas indicate those regions of the initial phase giving rise to dissociative trajectories, in which the action cannot be defined in the usual way. N, D, and R indicate nonreactive, dissociative, and reactive regions, respectively. The trajectories were begun with the distance from atom A to the center mass of BC being 12 bohr.

pares plots of the actions of the diatomic molecule at the end of the trajectory as a function of initial phase at a sequence of energies.[10(a),12,20,21] At energies above dissociation, one cannot calculate the action in the usual way, and one is left with gaps in the action vs phase plots. Examples of these plots are shown in Figs. 7 and 8 for the highest energies studied (reagent translational energies of 0.388 eV for $v = 0$ and 0.2815 eV for $v = 1$). Solid lines are used to indicate nonreactive processes and dashed lines are used to indicate reactive ones. The shaded regions mark those regions of initial phase in which the trajectories are dissociative and hence no action can be defined. In both of these figures, the dissociation is seen to occur between regions of high final action in reactive and nonreactive collisions (the maximum allowable final action in this system is 1.981, which is related to the fact that it only supports two bound states). This is quite reasonable behavior, as for dissociation to occur there must be more than the dissociation energy present in each diatomic molecule. Hence, the transition between reactive or nonreactive regions is expected to occur where the final action of the diatomic molecule equals its maximum value.

A somewhat different behavior is shown in Fig 9, in which we plot the final action vs initial phase in a collision

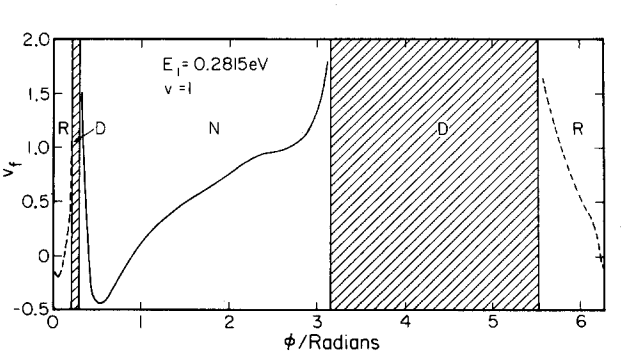

FIG. 8. Final action v_f as a function of initial phase Φ for a collision involving vibrationally excited molecules at a reagent translational energy E_i of 0.2815 eV. All markings are as in Fig. 7.

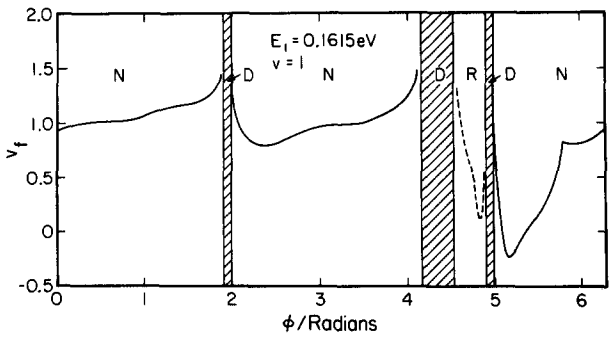

FIG. 9. Final action v_f as a function of initial phase Φ for a collision involving vibrationally excited molecules at a reagent translational energy E_1 of 0.1615 eV. All markings are as in Fig. 7.

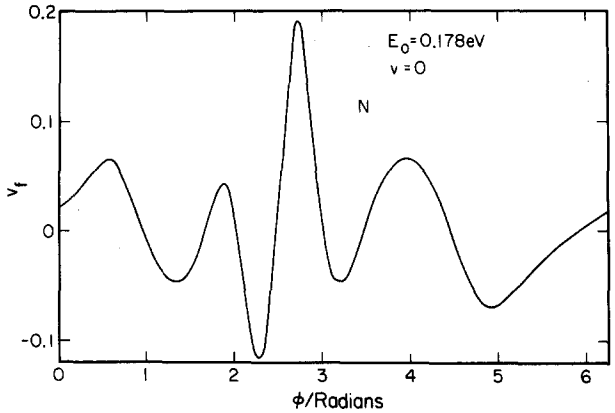

FIG. 10. Final action v_f as a function of initial phase Φ for a collision involving ground state molecules at a reagent translational energy E_0 of 0.178 eV. All markings are as in Fig. 7. Note the expanded scale of the ordinate.

with $v = 1$ reagent and a reagent translational energy of 0.1615 eV. Here there are three dissociative regions. Two are found between the reactive and nonreactive initial phase segments, and one is in the middle of the large nonreactive segment. The latter is part of the small dissociative band located near 2 rad initial phase between 0.15 and 0.20 eV initial reagent translational energy in Fig. 5 (and enlarged in Fig. 6). As the initial phase for reactive trajectories is varied so it closely approaches that in the dissociative region, the final action increases, suggesting that the consideration of dissociation as a limiting case of vibrational excitation is an appropriate concept.

There is a substantial difference between the product state distribution in collisions with $v = 1$ reagent at initial relative energies of 0.2815 eV (Fig. 8) and at 0.1615 eV (Fig. 9). At the higher energy, the likelihood of vibrational deexcitation, as measured by the large region of initial phase over which the final action is substantially smaller than one, is significantly greater than at the lower energy. At the lower energy, from $\Phi = 0$ to the second dissociative segment (at 4.15 rad), the final action never becomes smaller than 0.8. Thus, increasing translational energy seems to lead to increasing vibrational nonadiabaticity in nonreactive collisions. The small likelihood of reaction in these high translational energy regions makes it difficult to draw any conclusions concerning that process. A similar trend has been observed in the exact quantum mechanical calculations on this system.[22]

Further evidence of the tendency towards vibrational adiabaticity at low energies can be seen by considering a collision with $v = 0$ molecules at an energy (0.178 eV initial translational energy) at which only nonreactive collisions occur—no dissociation or reaction was found. A plot of the final action as a function of initial phase for this collision is given in Fig. 10. The near adiabaticity may be seen by noting that the total range of final actions in the figure is from -0.12 to 0.19, corresponding to final vibrational energies of 0.0639 and 0.1079 eV, respectively (the zero point energy of the diatomic reagent is 0.0818 eV). Hence, at most 15% of the initial translational energy was converted to vibrational energy in the collision. Another interesting feature of this figure is its relatively complicated structure. In spite of the fact that all collisions are nonreactive and nearly adiabatic, there is still a strong variation in the dependence of the final action on the initial phase.

To indicate what happens when the boundary regions between the reactivity bands become blurred, we present in Fig. 11 a plot of final action vs initial phase for the collision with a $v = 1$ molecule at a relative translational energy of 0.085 eV for initial phases in the range 2.40–3.10 rad. In this region one sees five separate dissociative segments, four of which occur between 2.50 and 2.70 rad. These may be thought of as being distinct from the larger dissociative segment between 2.90 and 3.10 rad. The latter band is part of the large dissociative band seen in the lower right-hand portion of Fig. 5. The action vs initial phase curves are fairly smooth between the dissociative segments. Away from the lower tip of the large dissociation and reaction band in Fig. 5, the boundaries are smoother. Figure 11 seems to represent, then, an upper limit to the complexity of such a diagram.

We next consider the partitioning of kinetic energy among the three atoms in dissociative collisions and also among the final atoms and diatom in reactive and nonreactive collisions. In all cases the collision partners are A and BC. The calculation of the energy partitioning fraction f_X has been described in Sec. II. Plots of these quantities as a function of the initial phase are shown in Figs. 12–17 for

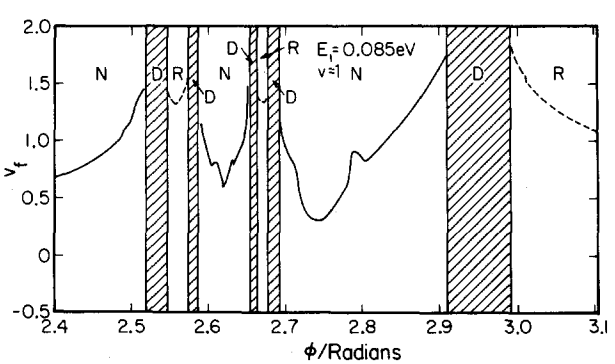

FIG. 11. Final action v_f as a function of the initial phase Φ for a collision involving vibrationally excited molecules at a reagent translational energy E_1 of 0.085 eV. The initial phases are limited to the chattering regions described in the text and the regions of slightly lower and higher initial phase. All markings are as in Fig. 7.

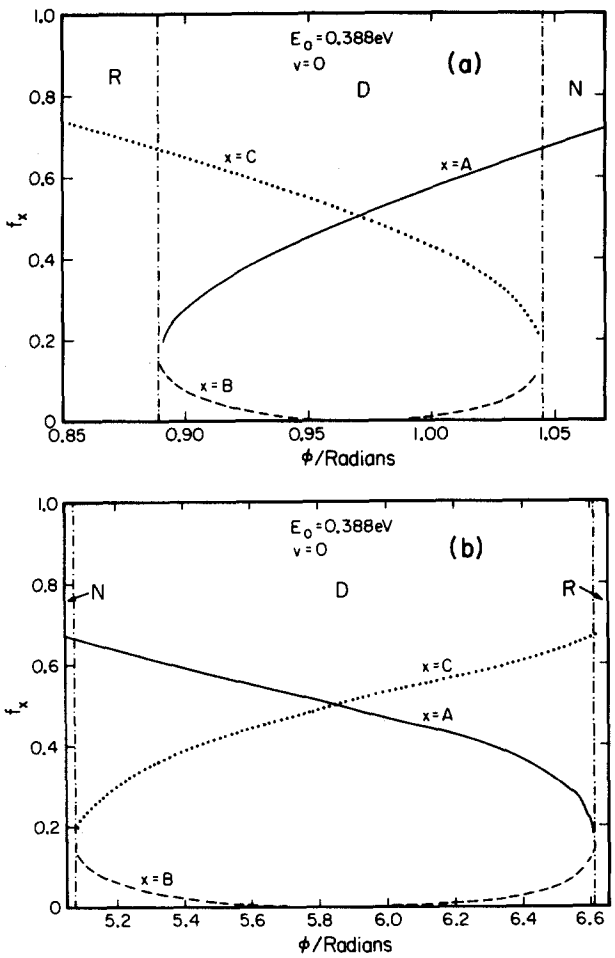

FIG. 12. Final energy fractions f_X(X = A, B, C) (defined in Sec. II) as a function of the initial phase Φ for the dissociative bands seen in collisions of ground state molecules at a reagent translational energy E_0 of 0.388 eV. A solid line is used for atom A, a dashed line for atom B, and a dotted line for atom C. A dashed–dotted line marks the approximate boundary between bands. The curve for atom A is continued into the nonreactive region and the curve for atom C is continued into the reactive region by a procedure described in the text. (a) The small band from 0.90 to 1.03 rad initial phase; (b) the large band from 5.10 to 6.60 rad.

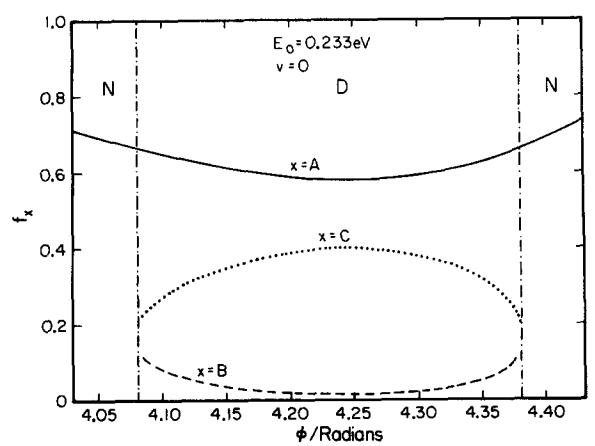

FIG. 13. Final energy fractions f_X as a function of initial phase Φ for dissociative bands in collisions of ground state molecules at a reagent translational energy E_0 of 0.233 eV. All markings are as in Fig. 12.

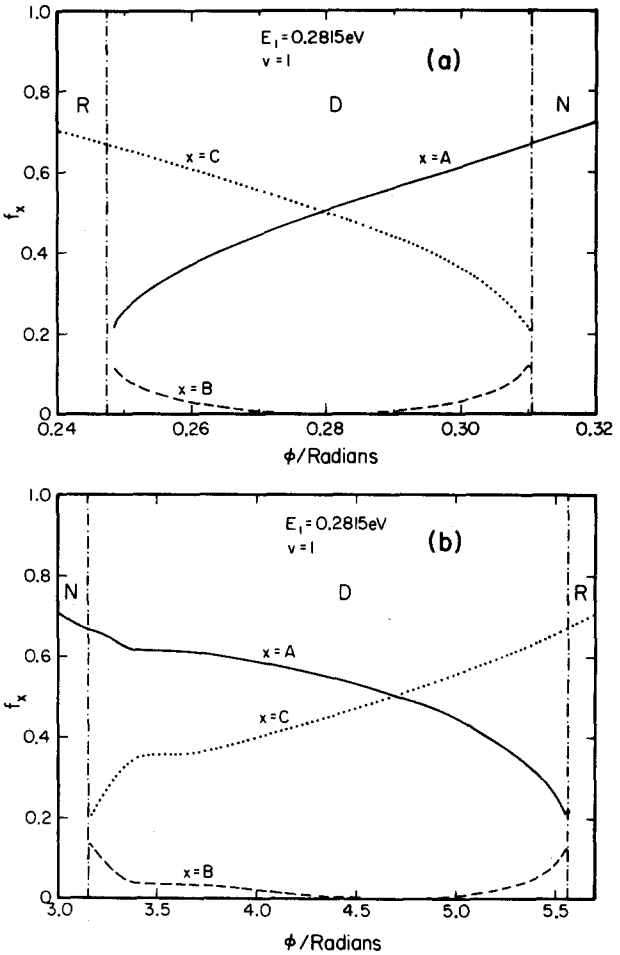

FIG. 14. Final energy fractions f_X as a function of initial phase Φ for dissociative bands in collisions of vibrationally excited molecules at a reagent translational energy E_1 of 0.2815 eV. (a) The small band from 0.25 to 0.31 rad; (b) the large band from 3.20 to 5.50 rad. All markings are as in Fig. 12.

initial phases near which dissociation occurs for a variety of initial conditions. A few important features are observed in these figures, and we review these here.

First, the curves are quite smooth in the dissociation regions. At the border between reactive and dissociative collisions, f_C smoothly matches onto the f_C^R curve, and at the border between nonreactive and dissociative collisions, f_A smoothly matches onto the f_A^N curve. In all cases, the matching occurs at a value of the energy fraction of 2/3; this is the maximum value f_A or f_C can take in the dissociative region for a system of three equal masses. The small values of f_B are also a requirement of the mass combination (for the case of three equal masses, f_B is required to be smaller than 1/6).

Second, two types of partitioning curves are seen. For those dissociative bands confined between one reactive and one nonreactive band, f_A and f_C must both have regions where they are large ($\approx 2/3$) and small ($\approx 1/6$). For those bands confined between two nonreactive bands, the f_A vs phase curve must have a minimum. The presence of such a minimum will have a major effect on the partitioning probabilities to be presented below. In principle, one might obtain

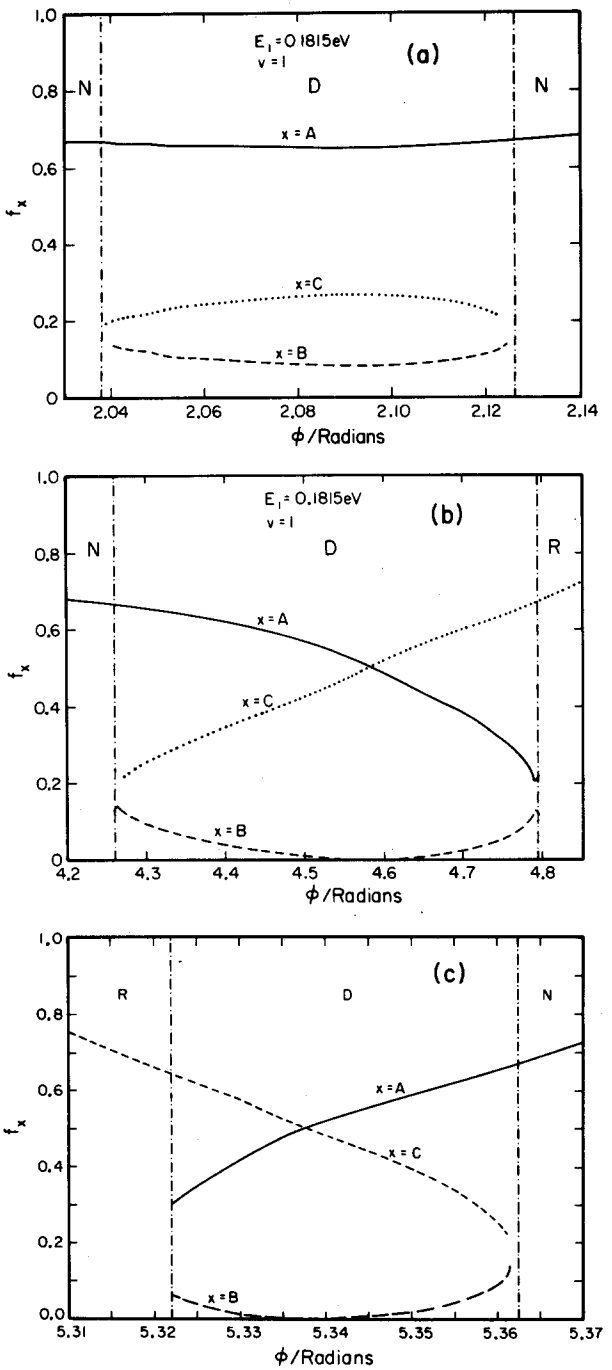

FIG. 15. Final energy fractions f_X as a function of initial phase Φ for dissociative bands in collisions of vibrationally excited molecules at a reagent translational energy E_1 of 0.1815 eV. (a) band from 2.04 to 2.12 rad; (b) band from 4.25 to 4.80 rad; (c) band from 5.32 to 5.36 rad. All markings are as in Fig. 12.

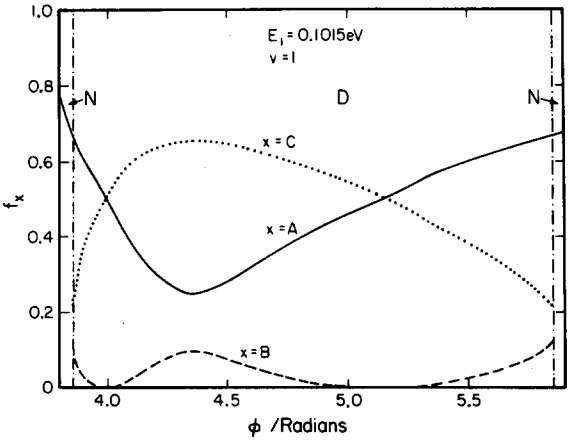

FIG. 16. Final energy fractions f_X as a function of initial phase Φ for dissociative bands in collisions of vibrationally excited molecules at a reagent translational energy E_1 of 0.015 eV. All markings are as in Fig. 12.

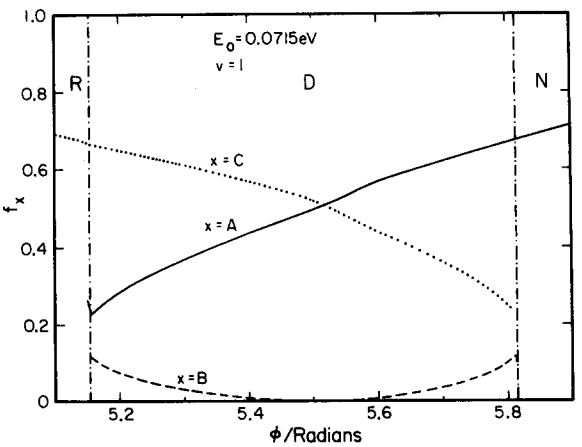

FIG. 17. Final energy fractions f_X as a function of initial phase Φ for dissociative bands in collisions of vibrationally excited molecules at a reagent translational energy of E_1 of 0.0715 eV. All markings are as in Fig. 12.

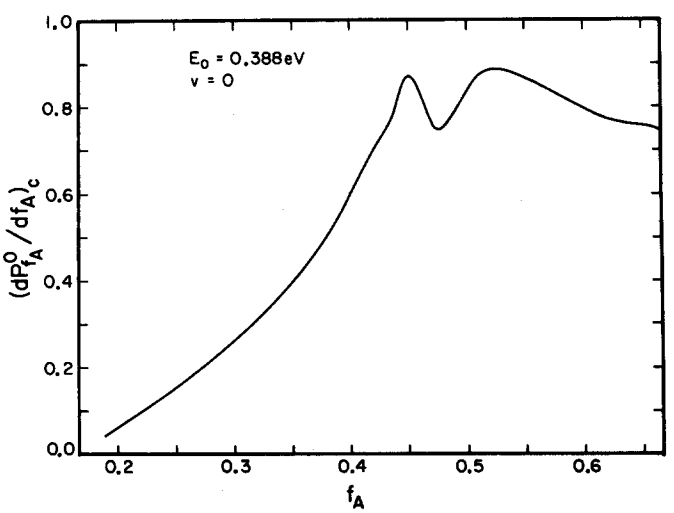

FIG. 18. Partitioning probability $(dP^0_{f_A}/df_A)_c$ (see Sec. II) as a function of energy fraction f_A of atom A for dissociation in collisions of ground state molecules at a reagent translational energy E_0 of 0.388 eV.

dissociative bands confined between two reactive ones, but such bands have not yet been observed.

Finally, we present results for the partitioning probability $(dP^v_{f_A}/df_A)_c$ defined in Sec. II. These are shown in Figs. 18–23 for the six sets of initial conditions for which energy fractions were shown as a function of initial phase in Figs. 12–17. The partitioning probabilities in the first and last of the former figures are compared with the corresponding quantum mechanical ones elsewhere.[7(d)] As mentioned pre-

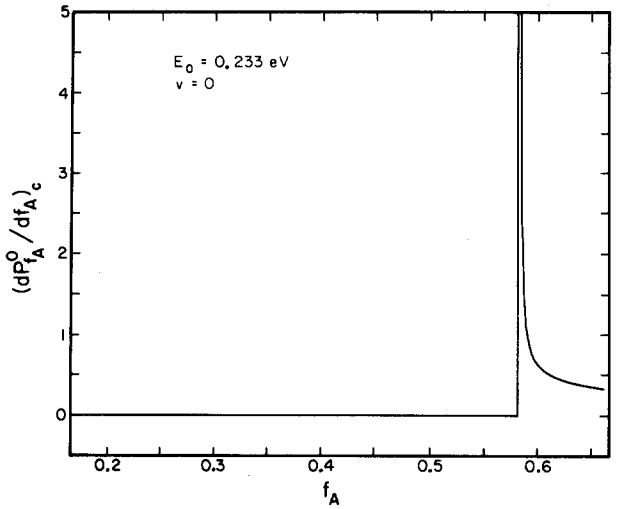

FIG. 19. Partitioning probability $(dP^0_{f_A}/df_A)_c$ as a function of energy fraction f_A for atom A for dissociation in collisions of ground state molecules at a reagent translational energy E_0 of 0.233 eV. The probability is zero for values of the energy fraction f_A below that at which it diverges ($\approx$0.58).

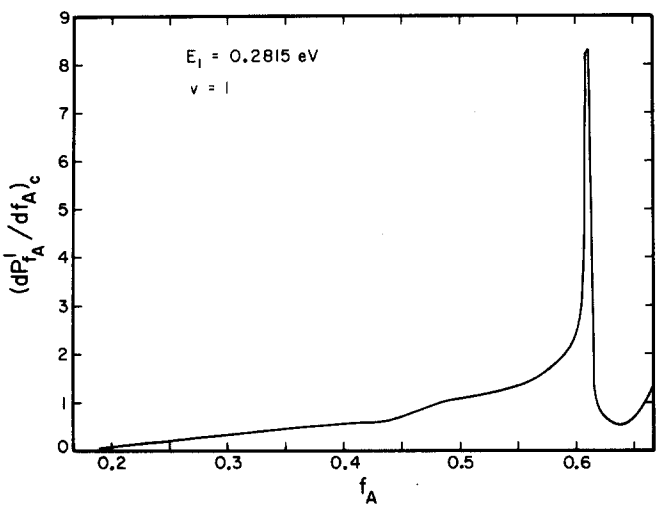

FIG. 20. Partitioning probability $(dP^1_{f_A}/df_A)_c$ as a function of energy fraction f_A for atom A for dissociation in collisions of vibrationally excited molecules at a reagent translational energy E_1 of 0.2815 eV.

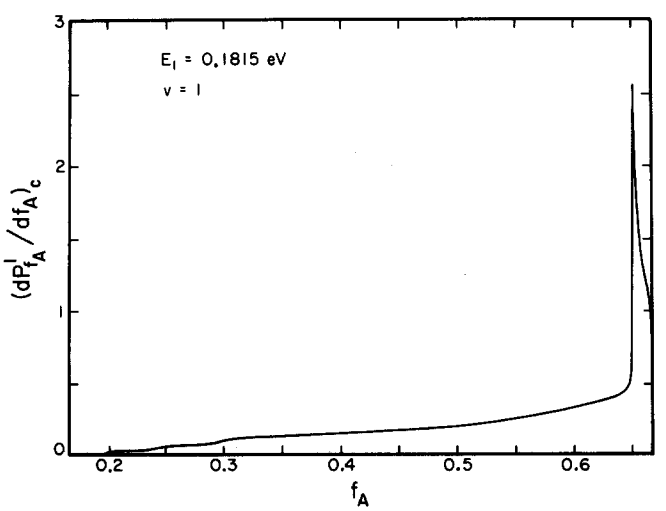

FIG. 21. Partitioning probability $(dP^1_{f_A}/df_A)_c$ as a function of energy fraction f_A for atom A for dissociation in collisions of vibrationally excited molecules at a reagent translational energy E_1 of 0.1815 eV.

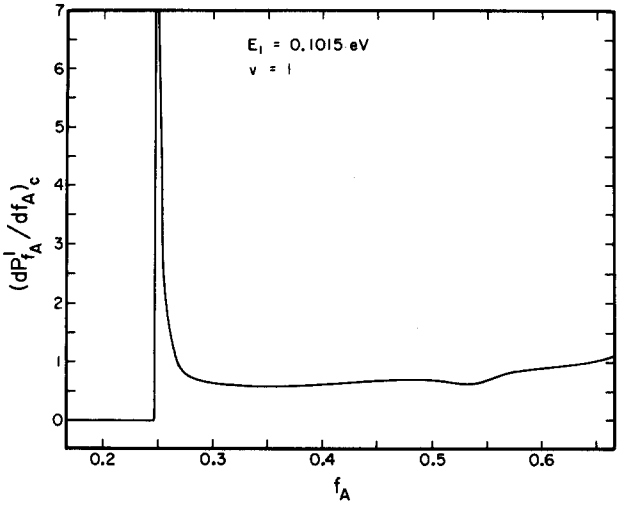

FIG. 22. Partitioning probability $(dP^1_{f_A}/df_A)_c$ as a function of energy fraction f_A for atom A for dissociation in collisions of vibrationally excited molecules at a reagent translational energy of 0.1015 eV. The probability is zero for values of the energy fraction f_A below that at which it diverges ($\approx$0.25).

viously (see Sec. II), there are some numerical difficulties involved in generating these curves, due to the necessity of interpolating and differentiating the f^D_X vs phase curves, as well as in obtaining highly accurate f^D_X values in regions where it is nearly independent of phase, thus making a major contribution to $(dP^v_{f_A}/df_A)_c$ as can be seen from Eq. (3). The details of the curves are less certain (and of less interest) than their broad, overall shape, which is expected to be less sensitive to numerical methods. They all appear quite different from each other, and we can rationalize much of their form simply from the reaction and dissociation probabilities, the kinematics of the system, and the existence of well-defined dissociation bands in the reactivity band plots (Figs. 4–6). We will consider this issue in greater detail in Sec. IV.

There are a few features of Figs. 18–23 which will prove to be of most interest. First is the tendency of the partitioning

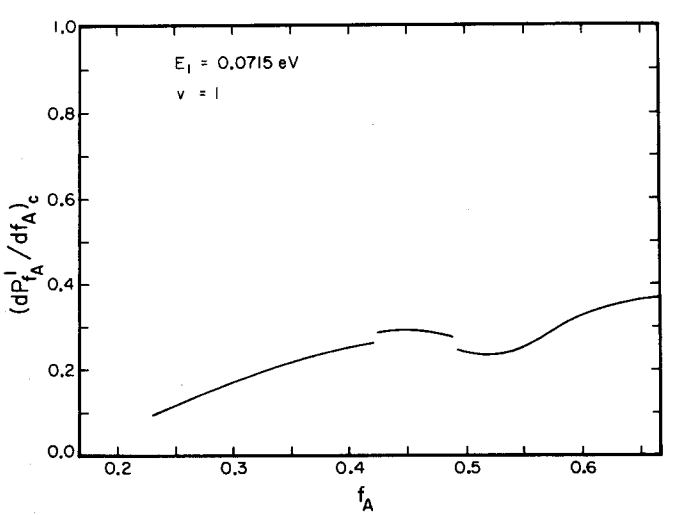

FIG. 23. Partitioning probability $(dP^1_{f_A}/df_A)_c$ as a function of energy fraction f_A for atom A for dissociation in collisions of vibrationally excited molecules at a reagent translational energy of 0.0715 eV.

probabilities to have their maxima near the maximum allowable energy fraction of 2/3, although this is not uniformly true (see particularly Fig. 22, in which the partitioning probability diverges at an $f_A = 0.25$). Second, in four out of the six cases studied, the partitioning probability either has poles (Figs. 19 and 22) or sharp peaks (Figs. 20 and 21).

IV. DISCUSSION

In this section we consider first the implication of the bandedness of dissociative trajectories as seen in the reactivity band plots (Figs. 4–6). In particular, we will focus on how this bandedness, when coupled with the calculated reaction probabilities and the kinematics of the collision, can be seen to lead to the general structure of the partitioning probability curves, such as those shown in Figs. 18–23. We then consider the origins of the bandedness of the dissociative trajectories and show that a close relationship can be established between the separate bands and different types of trajectories leading to dissociation.

A. Implications of the dissociative reactivity bands

Trajectories which lead to dissociation have been found to occur, as a general rule, in well-defined bands in the reactivity band plots (Figs. 4–6). Exceptions to this trend are found for collisions of a $v = 1$ molecule in which the reagent translational energy is in the range from 0.07 to 0.10 eV. In this region, the trajectory outcome may vary substantially with small changes in the initial phase of the diatomic molecule. This is somewhat reminiscent of the observation of chattering regions in the final action vs initial phase plots seen in reactive atom–diatomic collisions (at energies well below dissociation), particularly the $H + H_2$,[13,20(a)] $F + H_2$,[19,21] and $Cl + HCl$[23] reactions. Unlike in those cases, where the outcome of the trajectory appears to be random, seemingly smooth (but quite short) curves of final action vs initial phase can be obtained by the use of sufficiently small grid spacing (0.002 rad).

In most cases, dissociative trajectories can be thought of as limiting cases of reactive or nonreactive collisions giving rise to vibrational excitation of products. This can be seen in two interrelated ways. For values of the initial phase only slightly different from those of the trajectories which lead to dissociation, the diatomic molecules remaining at the end of the collision will be highly vibrationally excited. If one considers the fractional energy as a function of initial phase, such as that plotted in Figs. 11–17, one sees that the curve of atom A smoothly matches onto that for atom A in nonreactive collisions and that for atom C smoothly matches onto that for atom C in reactive collisions.

The nature of the dissociative segment (defined by the type of nondissociative segments between which it is confined at a given energy) will play a major role in determining the appearance of the partitioning probability curves. If the dissociative segment is confined between one reactive and one nonreactive segment, the partitioning probability curve should cover essentially all the accessible regions of energy fractions (1/6–2/3 in this case). If, on the other hand, the segment is confined between two nonreactive or two reactive ones, the partitioning probability curves will cover only a subset of the allowable energy fractions and must have at least one place where they diverge. This divergence occurs at values of f_A for which the f_A vs initial phase curves show extrema, as can be seen from Eq. (3). For the simplest case in which the dissociative segment is confined between two nonreactive segments, the divergence will occur at a minimum of f_A, and the dissociation probability below the singularity will vanish while above the singularity, it is continuous. Such curves are observed in Figs. 19 and 22. For the other simple case, a maximum in f_A will occur and the dissociation probability will vanish above the singularity and be continuous below it. Trajectories corresponding to this case have not been observed in the present system. More complicated situations might arise. More generally, one may, in principle, find curves of f_A vs ϕ for dissociative segments confined between two nonreactive ones having $n + 1$ minima and n maxima (leading to $2n + 1$ divergences in partitioning probability curves). Similarly, for dissociative bands confined between two reactive ones, there may be $n + 1$ maxima and n minima. No such curves (multiple minima and maxima) were observed, however.

These figures demonstrate that the value of the energy fraction at which the partitioning probability diverges can be quite close to its maximum or minimum permitted value. Precisely at what values of the energy fraction the partitioning probability diverges will depend on the shape of the dissociation and reaction reactivity bands at the energy being considered. If for instance, one is at an energy fairly near the onset of the reaction band, the minimum in the energy fraction vs phase plot will occur at a value of the energy fraction close to 1/6. This is the case in Fig. 22 (for which the important reaction and dissociation reactivity bands may be seen in Fig. 5). If the energy is such that one is not close to the onset of the reaction band, the minimum will occur at values of the energy fraction close to 2/3.

These discontinuities are very similar in appearance to those associated with rainbow scattering observed in the classical scattering of a particle by a spherically symmetric potential.[24] In that problem, the differential cross section is zero on the high angle side of the rainbow, while it has a smooth dependence on the deflection angle or the low angle side. These rainbows are analogous to the discontinuities here because the partitioning of the energy among the atomic products of CID is related to the asymptotic orientation of the classical trajectory with respect to the coordinate axes when plotted in the usual Delves mass-weighted coordinate system.[7(b)]

Certain types of curves of energy fraction vs phase in dissociative collisions which might in principle occur have not been observed in these studies. For instance, in no cases were curves with more than one minimum or maximum obtained. Hence, the partitioning probability diverges at one and only one energy fraction if it diverges at all. As mentioned earlier, no dissociative bands confined between two reactive bands were observed. Such bands would lead to partitioning probability plots opposite to those in Figs. 19 and 22: at all energy fractions above that at which the singularity occurs the probability would vanish. There seems to be no

reason why such bands should not exist, so we assume that their absence is a function of the particular potential energy surface and mass combination used.

The fact that reactive processes are less probable than nonreactive ones at the energies studied suggests that in dissociative collisions one may be more likely to find kinetic energy distributions in which atom A has the greatest portion of the available energy. This would give rise to the partitioning probability being dominated by high energy fractions. The range of energy fractions allowable is kinematically determined simply by the masses of the colliding particles, are given in Eqs. (5), which explains why only certain numerical regions of the energy fraction are allowed. Changing the masses would, therefore, change the partitioning probabilities of both kinematic and dynamic reasons.

The structure of the reactivity band plot differs very strongly for $v = 0$ and $v = 1$ molecule collisions, and this fact, coupled with the definite manner in which the position and width of the reactivity bands have been shown to determine the partitioning probabilities, suggest that one might obtain substantially different kinetic energy distributions from dissociation from the two reagent states at the same total energy. The same statement applies to translational energy. The simplest way of obtaining such different behaviors would be to locate an energy at which the dissociation from $v = 0$ occurs totally from a band which is confined between two nonreactive bands, while that from $v = 1$ occurs from one or more bands confined between one reactive and one nonreactive band. Thus, not only may the outcome of the collision (reaction, nonreaction, or dissociation) depend on the initial state, but the intimate details of dissociation may also be a function of the initial state.

B. Origin of the dissociative reactivity bands

Formation of reactivity bands in atom–diatomic molecule collisions has been observed in a variety of systems at energies below dissociation[12,13,20(a)]; banding has also been observed in a nonreactive system studied at energies above dissociation.[10(a)] The present paper is, to our knowledge, the first reactivity band study of dissociation in a reactive system. To explain the origin of reactivity bands, we are interested in understanding the nature of the trajectories which comprise each band. In particular, we focus on two questions. First, we want to know whether each separate band corresponds to different types of trajectories. Second, we want to know what happens near the boundaries between bands, especially in the chattering regions, such as that shown in Fig. 11, in which the outcome of the trajectory is extremely sensitive in the initial conditions of the trajectory.

Wright and Tan[12(c)] have shown in their study of the collinear T + HT system on the SSMK surface[25] that the two lowest energy reaction reactivity bands are comprised of different types of trajectories. In the lower energy band, reactive trajectories cross the symmetric stretch line only once, while in the higher energy band, they cross the symmetric stretch line three times. Representative trajectories are shown in Fig. 8 of Ref. 12(c). A similar correspondence can be drawn between the two reaction regions in Fig. 5 for collisions in which the diatom is initially in the $v = 1$ state. For the $v = 0$ case we show in Fig. 4 only the high energy reaction region; there is another one at lower energies responsible for the large values of P_0^R seen in Fig. 2. Trajectories comprising the lower reaction band in the $v = 1$ case cross the symmetric stretch line once (Fig. 24) while those in the higher band cross it three times (Fig. 25). Reactive trajectories must cross the symmetric stretch line an odd number of times; thus, these are the simplest kind of reactive trajectories possible. The same behavior is seen in collisions of ground state molecules; we do not show them here.

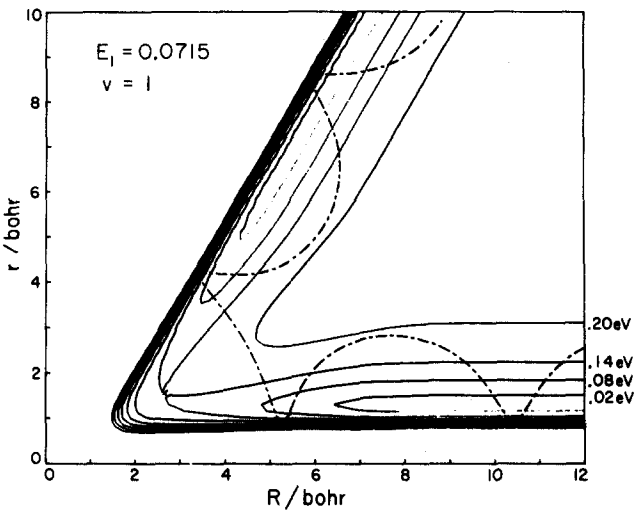

FIG. 24. Plot of typical reactive trajectory in the low energy reaction reactivity band for collisions of a vibrationally excited molecule. The trajectory is for an initial translational energy of 0.0715 eV and initial vibrational phase of 3.4558 rad. The integration of the trajectory was begun with $R = 12.8952$ bohr. The trajectory is superimposed on a plot of the potential energy surface for the system in Delves mass-scaled coordinates. Contours are drawn every 0.06 eV starting from 0.02 up to 0.50 eV with respect to the bottom of the well of the isolated diatomic molecule. The × marks the saddle point for the reaction. Note that there is only one crossing of the symmetric stretch line.

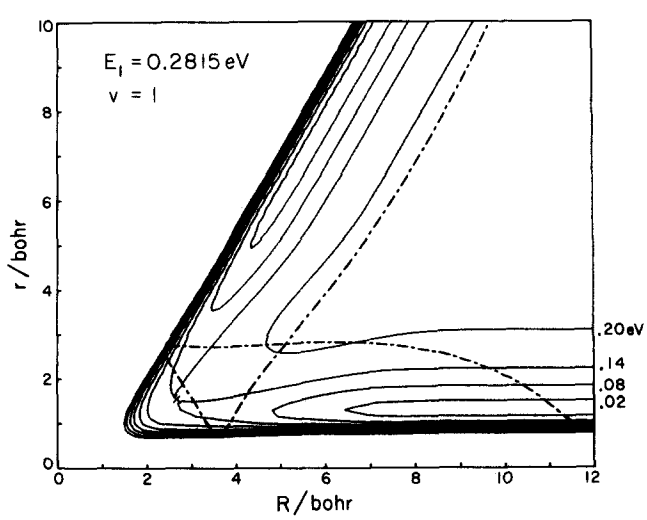

FIG. 25. Plot of a typical reactive trajectory in the high energy reaction reactivity band for collisions of vibrationally excited molecules. Trajectory is for initial translational energy of 0.2815 eV and initial vibrational phase of 0.2817 rad. All markings are as in Fig. 24.

We next consider the nature of trajectories leading to dissociation. We focus our attention first on the single dissociation band (Fig. 4) for collisions of ground state molecules and two large bands (Fig. 5) for collisions of $v = 1$ molecules. We consider the small band for $v = 1$ isolated in the large nonreactive band and the overall chattering region later. Typical dissociative trajectories are shown in Figs. 26–28 for the dissociative band in $v = 0$ collisions, the first dissociative band in $v = 1$ collision, and the second such band in $v = 1$ collisions, respectively. In Figs. 26 and 28, the trajectory crosses the symmetric stretch line three times; in Fig. 27 the symmetric stretch line is crossed only once. The three crossings for Figs. 26 and 28 are associated with two internal collisions in the strong interaction region, the first between A and B and the second between B and C. For Fig. 27 the single crossing of the symmetric stretch line is also associated with two internal collisions, but in inverse order, the first between B and C and the second between A and B. This suggests that the separate dissociation bands are each comprised of trajectories crossing the symmetric stretch line a different number of times, just as was seen for reactive transitions. Andrews and Chesnavich[14(b)] have also noted that dissociative trajectories may originate on either side of the symmetric stretch line in symmetric (A–B–A) systems. Compared to the reactive case, things are not quite so simple in the dissociation case, however, as the trajectory need not cross the symmetric stretch line an odd number of times. In fact, trajectories which cross it twice have been observed in both of the $v = 1$ reactivity bands. The last crossing of the symmetric stretch line may occur (as does that in the trajectory shown in Fig. 27) at large values of the internuclear coordinates. Whether or not such a crossing takes place will depend on the partitioning of the energy among the three atoms. The final crossing may be thought to occur while the atoms are in the process of dissociating, even if the crossing occurs at fairly small values of the internuclear coordinates. Thus, the first dissociation reactivity band in the reactivity plot (in Fig. 5) may be thought of as being comprised of trajectories which cross the symmetric stretch line once prior to the process of actually dissociating (during which they may again cross that line). In the second dissociation band for $v = 1$ and the only such band for $v = 0$, two crossings take place prior to the onset of dissociation, after which a third crossing may occur.

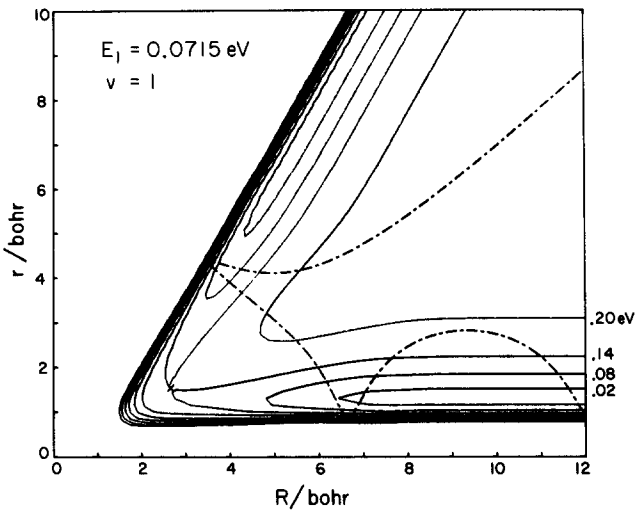

FIG. 27. Plot of a typical dissociative trajectory in the low energy dissociation reactivity band for collisions of vibrationally excited molecules. Trajectory is for initial translational energy of 0.0715 eV and initial vibrational phase of 5.3407 rad. All markings are as in Fig. 24.

These observations allow one to make a simple physical picture to account for the observed vibrational enhancement of CID in this system. The simplest trajectory which may lead to dissociation does not occur when the molecule is in its ground state. It occurs when the molecule is in its excited state. Since more complicated trajectories appear to contribute only at higher energies, low energy dissociation is prevented in the ground state case. The qualitative agreement between the quasiclassical trajectory calculations and the exact quantum ones reported previously[7] indicate that this simple classical picture may be a reasonable one to use in

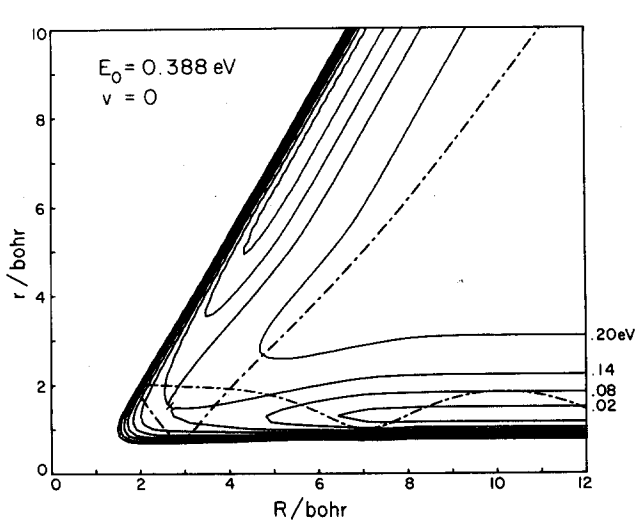

FIG. 26. Plot of a typical dissociative trajectory in collisions of ground state molecules. Trajectory is for initial translational energy of 0.388 eV and initial vibrational phase of 0.3142 rad. All markings are as in Fig. 24.

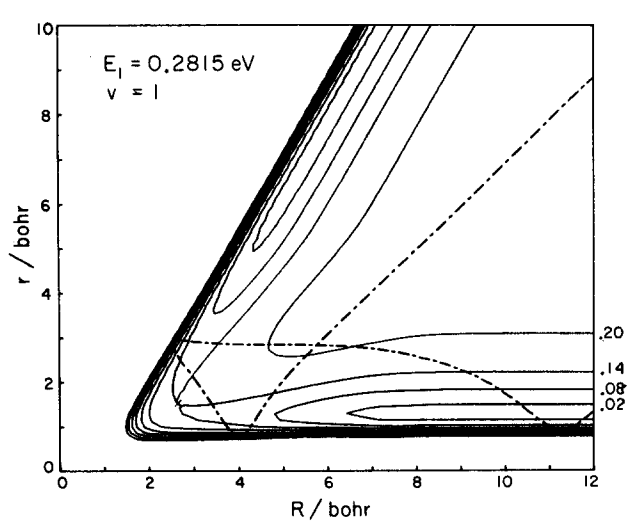

FIG. 28. Plot of a typical dissociative trajectory in the large, high energy dissociation reactivity band for collisions of vibrationally excited molecules. Trajectory is for initial translational energy of 0.2815 eV and initial vibrational phase of 5.3407 rad. All markings are as in Fig. 24.

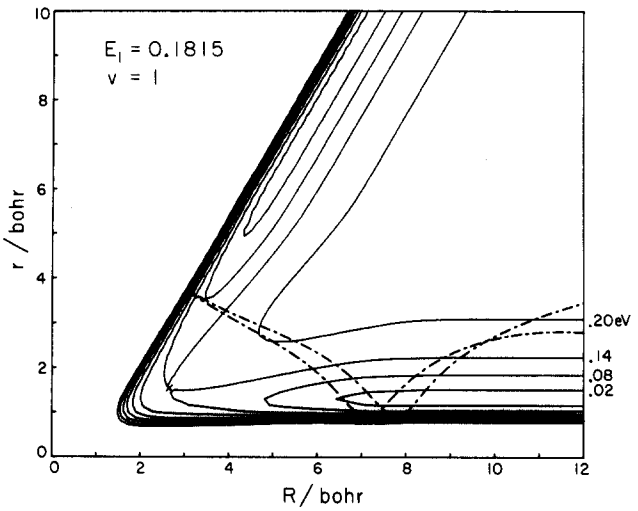

FIG. 29. Plot of a typical dissociative trajectory in the small dissociation reactivity band imbedded in the large nonreaction band for the collision of a vibrationally excited molecule. Trajectory is for initial translational energy 0.1815 eV and initial vibrational phase of 2.12 rad. All markings are as in Fig. 24.

attempting to understand the calculated vibrational enhancement of CID in this system.

We next wish to consider the small dissociation band seen in Fig. 5 (and enlarged in Fig. 6) near 2 rad and 0.18 eV reagent translational energy. A typical trajectory for this band is shown in Fig. 29. This trajectory is quite different from the dissociative ones seen in Figs. 26 and 28. This should not be surprising, however, and this small dissociative band is imbedded in a large nonreactive band and the other dissociative bands tend to be confined between reactive and nonreactive bands. Examination of nonreactive trajectories near the boundaries between the nonreactive and dissociative reactivity bands indicates that differences between the trajectories within them are quite small and become important only at large values of the internuclear coordinates.

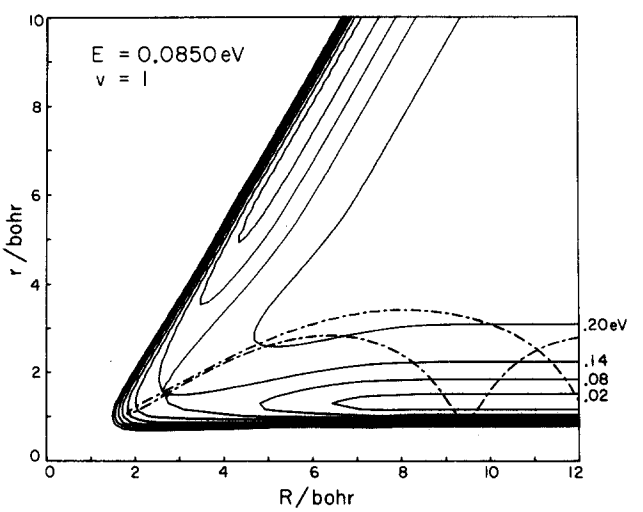

FIG. 30. Plot of a nonreactive trajectory for the collision of a vibrationally excited molecule in the chattering region shown in Fig. 11. Trajectory is for an initial translational energy of 0.085 eV, and an initial phase of 2.65 rad. All markings are as in Fig. 24.

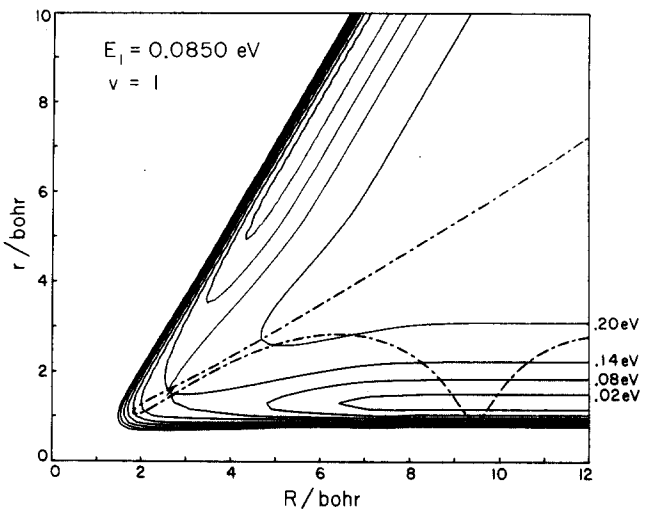

FIG. 31. Plot of a dissociative trajectory in the chattering region shown in Fig. 11. Initial conditions are the same as for the trajectory in Fig. 29, except that the initial vibrational phase is 2.66 rad. All markings are as in Fig. 24.

This is a case then, in which the final outcome of the trajectory is not seen until well after the collision might be thought to be finished (R_{AB} large and increasing, R_{BC} fairly small).

We finally consider the chattering regions indicated in Fig. 11. In the regions of initial phase from 2.5 to 2.7 rad, the outcome of the trajectory varies greatly with small changes in the initial phase. Such regions have been observed in studies of reactions below dissociation, particularly the $H + H_2$[13,20(a)] and $F + H_2$[19,21] reactions. In these regions, the trajectories become very complicated, frequently bouncing back and forth many times in the strong interaction regions of the potential energy surface. Atom B is said to "chatter" between atoms A and C, hence the name chattering regions.

In this case, the trajectories in the chattering regions are not overly complicated. Three such trajectories are shown in Figs. 30–32 corresponding to initial conditions shown in Fig. 11. The initial phase differs by 0.01 rad (0.57°) between each

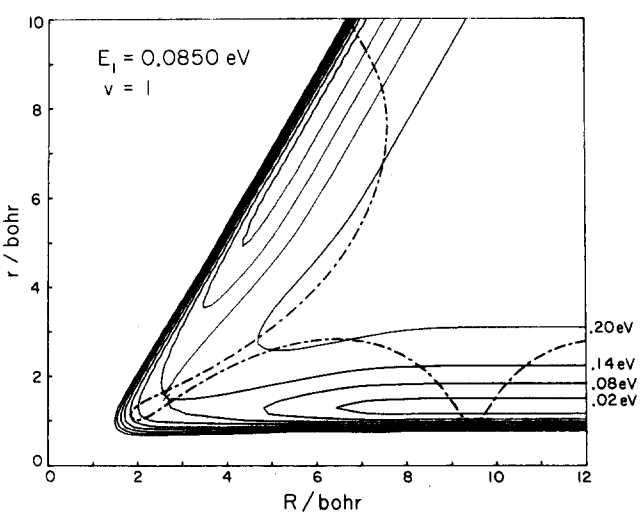

FIG. 32. Plot of a reactive trajectory in the chattering region shown in Fig. 11. Initial conditions are the same as for the trajectory in Fig. 30, except that the initial vibrational phase is 2.67 rad. All markings are as in Fig. 24.

trajectory. The dominant feature of the trajectories is clear: trajectories in this region involve motion more or less along the symmetric stretch line. The extreme sensitivity of the trajectory outcome to the initial phase can be rationalized as follows. In moving the symmetric stretch line, the trajectory can naively be viewed as having "forgotten" from where it was begun, and therefore it is reasonable that a small perturbation to the trajectory could seriously alter its course.

At energies below dissociation motion exactly along the symmetric stretch line would constitute that of a trapped trajectory—one which could oscillate back and forth forever, never leaving the interaction regions of the potential energy surface.[26] In the language of Pollak and Pechukas, such motion constitutes a trapped trajectory of the first kind.[27] These trajectories are frequently found at the boundary between reactive and nonreactive bands in atom–diatomic molecule systems at energies below dissociation.[12,13,21,22] At energies above dissociation, trapped trajectories of the first kind (in which the trajectory oscillates back and forth forever between the two different equipotential lines for the given total energy) do not exist. A trajectory can change its character continuously from reactive to nonreactive or vice versa by going through an intermediate stage of dissociative trajectories. Thus, the requirement shown by Pechukas and Pollak that trapped trajectories must occur at the boundary between reactive and nonreactive bands at energies below dissociation is not applicable at energies above dissociation.[25] Andrews and Chesnavich[14(b)] have, in fact, shown the necessity of having dissociative trajectories occurring with initial conditions between those of nonreactive and reactive trajectories. Nothing in these statements, however, precludes the possiblity of formation of trapped trajectories of the second or third kinds.[27] No such trapped trajectories (or nearly trapped ones) were observed, although we have not carried out a systematic search for them.

CONCLUSIONS

We have performed a reactivity band analysis of CID in a model collinear reactive atom–diatomic molecule system on which nonreactive, reactive, and dissociative processes are possible. Quasiclassical trajectories are believed to provide a reasonable view of the dynamics in this system because of the qualitative similarity in the reaction and dissociation probabilities calculated by trajectories and by exact quantum mechanical calculations.[7]

CID is shown to occur almost entirely in well-defined bands in initial phase–initial translational energy space, the exception being a small contribution from dissociative trajectories in a chattering region in which the outcome of the trajectory is extremely sensitive to the initial vibrational phase of the reagent molecule. Dissociation may be thought of as a limiting case of vibrational excitation, as nondissociative (reactive or nonreactive) trajectories with initial conditions only slightly different from those leading to dissociation result in a diatomic molecule product which is highly vibrationally excited. In most cases, dissociative reactivity bands found are confined between one reactive and one nonreactive band; in the rest, they may be found between two nonreactive bands. In no instances were dissociative bands confined between two reactive bands.

The partitioning of kinetic energy among the three atomic products of dissociative collisions was calculated and shown to be a smooth function of the initial phase throughout the dissociation band. Kinematic considerations require that most of the available kinetic energy go onto the end atoms (A or C). The fraction of the available kinetic energy in the end atoms, as a general rule, matches smoothly onto that of the free atom in nondissociative collisions (atom A in nonreactive collisions, atom C in reactive ones).

From the curves of final energy fraction vs initial phase we have been able to calculate the partitioning probability, that is, the likelihood of the dissociation process to distribute the available energy in a given way. Plots of the partitioning probabilities vs final energy fraction for six different sets of initial conditions (reagent vibrational state and translational energy) display a wide range of behavior. The general form of these partitioning probability curves can be inferred solely by examination of the reactivity band plots.

The different dissociative reactivity bands found for the reaction of vibrationally excited ($v = 1$) molecules have been shown to be comprised of different kinds of trajectories. The band which dominated at low energies (and ends at reagent translational energies about 50% above the dissociation energy) is seen to arise from trajectories which cross the symmetric stretch line only once prior to the onset of actual dissociation, while the higher energy band arises from trajectories which cross the symmetric stretch line an additional time. The single dissociation band observed in collisions of ground state molecules is seen to be made up of trajectories which cross the symmetric stretch line twice prior to dissociation. Hence, the vibrational enhancement of CID can be thought of as being due to the inability of ground state molecules to dissociate by the simplest possible trajectory; dissociation from such ground states is only possible by a more complex procedure, which only becomes important at higher energies.

The chattering region is seen to arise from trajectories which at some point follow the symmetric stretch line very closely. Since the available energy is greater than the dissociation energy, motion along the symmetric stretch line does not constitute a trapped trajectory. The existence of a dissociation channel allows for a smooth transition from reactive to nonreactive trajectories via an intermediate region of dissociative trajectories. As a result, trapped trajectories need not occur at the boundary between reactive and nonreactive trajectories.

Our analysis has been restricted to a single model of a potential energy surface for a collinear collision. In a reactive system, changes in the masses of the atoms have been shown to produce major changes in the structure of the reactivity bands.[12(b)] Exact quantum mechanical calculations on isotopically substituted versions of the model system studied here (mass combinations 10–1–10 and 1–35–1) indicate that the effect of mass on dissociation is strong.[24] Large changes in the reactivity band structure can be expected. Thus one must use caution in attempting to make generalizations on the basis of the reactivity bands for one system.

Removal of the collinearity restriction might be expected to lead to substantial changes in the reactivity bands. In studies of the two- and three-dimensional T + HT reaction, Wright[12(e)] has shown a disappearance of the bandedness observed in the collinear reaction, which is due to the diminished importance of multiple collisions (which involve multiple crossing of the symmetric stretch line) in noncollinear collisions. Thus, in three-dimensional systems, the richness of the banded structure obtained here might be expected to be substantially reduced.

ACKNOWLEDGMENTS

The calculations reported here were performed on the Dreyfus–NSF Theoretical Chemistry Computer which was funded through grants from the Camille and Henry Dreyfus Foundation, the National Science Foundation (Grant No. CHE-78-20235), and the Sloan Fund of the California Institute of Technology.

[1]R. L. Belford and R. A. Strehlow, Annu. Rev. Phys. Chem. **20**, 247 (1969).
[2]A. Dalgarno and W. G. Roberge, Astrophys. J. **233**, L25 (1979); D. Hollenbach and C. F. McKee, Astrophys. J. Supp. Ser. **41**, 555 (1979); W. Roberge and A. Dalgarno, Astrophys. J. **255**, 176 (1982).
[3]P. J. Kuntz, in *Atom–Molecule Collision Theory*, edited by R. B. Bernstein (Plenum, New York, 1979), pp. 669–692, and references therein.
[4](a) D. J. Diestler, in *Atom–Molecule Collision Theory*, edited by R. B. Bernstein (Plenum, New York, 1979), pp. 655–667, and references therein; (b) G. D. Barg and A. Askar, Chem. Phys. Lett. **76**, 609 (1980); (c) C. Leforestier, G. Bergeron, and P. C. Hiberty, *ibid.* **84**, 385 (1981); P. M. Hunt and S. Sridharan, J. Chem. Phys. **77**, 4022 (1982).
[5](a) I. Rusinek, J. Chem. Phys. **72**, 4518 (1980); (b) I. Rusinek and R. E. Roberts, *ibid.* **68**, 1147 (1978).
[6](a) K. C. Kulander, J. Chem. Phys. **69**, 5064 (1978); Nucl. Phys. A 353, 341c (1981); (b) C. Leforestier, Chem. Phys. **87**, 241 (1984).
[7](a) A. Kuppermann, J. A. Kaye, and J. P. Dwyer, Chem. Phys. Lett. **74**, 257 (1980); (b) J. A. Kaye and A. Kuppermann, *ibid.* **78**, 546 (1981); (c) J. P. Dwyer, Ph.D. thesis, California Institute of Technology, 1977; (d) J. A. Kaye and A. Kuppermann, Chem. Phys. Lett. **115**, 158 (1985).
[8](a) A. Hauke, J. Manz, and J. Römelt, J. Chem. Phys. **73**, 5040 (1980); (b) J. Manz and J. Römelt, Chem. Phys. Lett. **77**, 172 (1980).
[9]L. H. Beard and D. A. Micha, J. Chem. Phys. **73**, 1193 (1980).
[10](a) J. C. Gray, G. A. Fraser, and D. G. Truhlar, Chem. Phys. Lett. **68**, 359 (1979); (b) J. C. Gray, G. A. Fraser, D. G. Truhlar, and K. C. Kulander, J. Chem. Phys. **73**, 5726 (1980); (c) J. C. Gray and D. G. Truhlar, *ibid.* **76**, 5350 (1982).
[11]E. W. Knapp and D. J. Diestler, J. Chem. Phys. **67**, 4969 (1977).
[12](a) J. S. Wright, K. G. Tan, K. J. Laidler, and J. E. Hulse, Chem. Phys. Lett. **30**, 200 (1975); (b) J. S. Wright, K. G. Tan, and K. J. Laidler, J. Chem. Phys. **64**, 970 (1976); (c) J. S. Wright and K. G. Tan, *ibid.* **66**, 104 (1977); (d) K. G. Tan, K. J. Laidler, and J. S. Wright, *ibid.* **67**, 5883 (1977); (e) J. S. Wright, *ibid.* **69**, 720 (1978); (f) K. J. Laidler, K. G. Tan, and J. S. Wright, Chem. Phys. Lett. **46**, 56 (1977).
[13]R. E. Howard, A. C. Yates, and W. A. Lester, Jr., J. Chem. Phys. **66**, 1960 (1977).
[14](a) P. M. Hunt and M. S. Child, J. Phys. Chem. **86**, 1116 (1982); (b) B. K. Andrews and W. J. Chesnavich, Chem. Phys. Lett. **104**, 24 (1984).
[15]R. N. Porter and L. M. Raff, in *Dynamics of Molecular Collisions, Part B*, edited by W. H. Miller (Plenum, New York, 1976), pp. 1–52; D. G. Truhlar and J. T. Muckerman, in *Atom–Molecule Collision Theory*, edited by R. B. Bernstein (Plenum, New York, 1979), pp. 505–565.
[16]J. M. Bowman and A. Kuppermann, Chem. Phys. Lett. **34**, 523 (1975).
[17]H. Eyring, J. Walter, and G. Kimball, *Quantum Chemistry* (Wiley, New York, 1944), pp. 272–273.
[18]In Ref. 7(b), Eq. (8) implies erroneously that $f_{\Lambda}^{\min} = 0$.
[19]J. S. Hutchinson and R. E. Wyatt, J. Chem. Phys. **70**, 3509 (1979).
[20](a) J. W. Duff and D. G. Truhlar, Chem. Phys. Lett. **4**, 1 (1974); (b) J. R. Stine and R. A. Marcus, *ibid.* **29**, 575 (1974); (c) N. Sathyamurthy, *ibid.* **59**, 95 (1978); (d) M. S. Child and K. B. Whaley, Faraday Discuss. Chem. Soc. London **67**, 57 (1979).
[21]F. Schnabel and S. Chapman, Chem. Phys. Lett. **57**, 189 (1978).
[22]J. A. Kaye and A. Kuppermann (unpublished).
[23]J. A. Kaye, Ph.D. thesis, California Institute of Technology, 1982.
[24](a) H. Pauly and J. P. Toennies, Adv. At. Mol. Phys. **1**, 258 (1965); (b) E. A. Mason, J. Chem. Phys. **62**, 667 (1957).
[25]I. Shavitt, R. M. Stevens, F. L. Minn, and M. Karplus, J. Chem. Phys. **48**, 2700 (1968).
[26]P. Pechukas and E. Pollak, J. Chem. Phys. **67**, 5976 (1977).
[27]E. Pollak and P. Pechukas, J. Chem. Phys. **69**, 1218 (1978).